


Superconducting diode effect in quantum spin Hall insulator based Josephson junctionsBenedikt Scharf *Institute for Theoretical Physics and Astrophysics and Würzburg-Dresden Cluster of Excellence ct.qmats,
University of Würzburg, Am Hubland, 97074 Würzburg, Germany*Denis Kochan **Institute of Physics, Slovak Academy of Sciences, 84511 Bratislava, Slovakia
and Center for Quantum Frontiers of Research and Technology (QFort), National Cheng Kung University, Tainan 70101, Taiwan*Alex Matos-Abiague *Department of Physics & Astronomy, Wayne State University, Detroit, Michigan 48201, USA*

(Received 12 June 2024; revised 23 September 2024; accepted 25 September 2024; published 10 October 2024)

The superconducting diode effect (SDE) is a magnetoelectric phenomenon where an external magnetic field imparts a nonzero center-of-mass momentum to Cooper pairs, either facilitating or hindering the flow of supercurrent depending on its direction. We propose that quantum spin Hall insulator (QSHI)-based Josephson junctions can serve as versatile platforms for nondissipative electronics exhibiting the SDE when triggered by a phase bias and an out-of-plane magnetic field. By computing the contributions from Andreev bound states and the continuum of quasiparticle states, we provide both numerical and analytical results scrutinizing various aspects of the SDE, including its quality Q factor. The maximum value of the Q factor is found to be universal at low (zero) temperatures, which ties its origin to underlying topological properties that are independent of the junction's specific details. As the magnetic field increases, the SDE diminishes due to the closing of the induced superconducting gap caused by orbital effects. To observe the SDE, the QSHI-based Josephson junction must be designed so that its edges are transportwise nonequivalent. Additionally, we explore the SDE in a more exotic yet realistic scenario, where the fermionic ground-state parity of the Josephson junction remains conserved while driving a current. In this 4π -periodic situation, we predict an enhancement of the SDE compared to its 2π -periodic, parity-unconstrained counterpart.

DOI: [10.1103/PhysRevB.110.134511](https://doi.org/10.1103/PhysRevB.110.134511)**I. INTRODUCTION**

Magnetoelectric phenomena accompanying superconductors with broken time-reversal and space-inversion symmetries are attracting considerable attention [1]. There are numerous superconducting systems displaying the supercurrent diode effect (SDE) including (1) thin superconducting films [2–5]; (2) Josephson junctions (JJs) based on (i) semiconductors, [6–11], (ii) topological semimetals [12], (iii) proximity-magnetized metals with strong spin-orbit coupling (SOC) [13], (iv) van der Waals heterostructures, [14–16], (v) twisted bilayer [17] and trilayer [18] graphenes, (vi) high- T_c superconductors [19,20], (vii) ferromagnets [21], (viii) topological insulators [22–25] or semiconductor-based Majorana wires [26–28], (ix) spin-orbit coupled quantum dot junctions [29]; (3) Josephson weak links through a single magnetic atom [30]; or even (4) altermagnets [31,32]. As many of them demonstrate the potential for supercurrent rectification, that is, maintaining a system superconducting for one current direction, while transiting it to the resistive state for the opposite one, they digress in the roles played by mag-

netic fields, Meissner screening, magnetization, the origin of spin-momentum locking, and generically in the spin-resolved spectral properties of the associated subgap states. All these nuances diversify the SDE and pin its origin with various proliferating adjectives like intrinsic, trivial, universal [33], anomalous [34], ubiquitous [5], field free [15], single atomic [30], flux tunable [35], high temperature [20], altermagnetic [31], and transverse [36], among others.

There is a common agreement linking the SDE to the appearance of a finite center-of-mass momentum of Cooper pairs, although, there is less consensus on what causes its nonzero value. The breakdown of time-reversal symmetry, triggered by a magnetic field (via Zeeman coupling) or magnetization (via exchange splitting), and a moving condensate while probing the supercurrent seem to be necessary ingredients in all scenarios [5–7,9–11,33,37–48]. However, there is still an ongoing discussion to which extent the SOC plays a role. Since experiments vary in terms of materials, geometry, measurements, and even the nature of superconductivity (whether intrinsic or proximity induced), no single theory can comprehensively explain the SDE in all its various forms. The primary distinction between models of the SDE lies in their stance on SOC. Pro-SOC models [6,7,9,10,37–44,49,50] link supercurrent rectification to the emergence of a helical

*Contact author: denis.kochan@savba.sk

superconducting phase [37,38,51–54]. In contrast, con-SOC models [5,33,45,47,48] attribute the SDE either to a Doppler shift in the quasiparticle spectra for left and right movers or to diamagnetic effects resulting from stray fields and inhomogeneous screening, or alternatively to Yu-Shiba-Rusinov states [30,55].

In this paper we scrutinize magnetochiral properties of two-dimensional (2D) JJs based on quantum spin Hall insulators (QSHI) and explore their abilities to foster the SDE when tuning an out-of-plane magnetic field, the phase biasing, and/or the edge-channels asymmetry. We compute individual contributions to the supercurrent carried by the spin-resolved Andreev bound states (ABS) and the continuum quasiparticle states, and analyze their roles in the emergence of the SDE. Using a minimal yet realistic model capturing the main junction characteristics and considering the relevant system parameters, we investigate the SDE and provide practical analytical formulas for the underlying quality Q factor, focusing primarily on its dependencies on magnetic field and temperature. We show that in the presence of an out-of-plane magnetic field and at very low temperatures the maximum of the Q factor acquires a universal value, which is independent of the junction parameters. Finally, we show that the SDE and its corresponding Q factor can be further enhanced by considering 4π -periodic junctions where the fermionic ground-state parity remains conserved while probing the supercurrent, which requires a measurement of the SDE on timescales shorter than the quasiparticle poisoning time.

The paper is organized as follows: In Sec. II we present the model Hamiltonian and discuss the associated Andreev and continuous spectra and their corresponding density of states. In Sec. III we study the underlying free energy and Josephson current and their dependencies on temperature and magnetic field, among other junction parameters. The effects of the magnetic field, edge-state Fermi velocities, and temperature on the properties of the SDE and Q factor in QSHI-based 2D junctions are analyzed in Sec. IV. Section V is devoted to the discussion of the SDE when the fermionic ground-state parity is conserved. We examine possible ramifications toward experimental realizations of the SDE in QSHI-based JJs in Sec. VI. After the concluding remarks, the paper is supplemented with two brief technical Appendixes.

We use standard notations throughout this paper, where $e > 0$ stands for the elementary charge, $\Phi_0 = h/e$ is the quantum of the magnetic flux, and k_B is the Boltzmann constant. Additionally, $\Theta(x)$ and $\text{sgn}(x)$ denote the Heaviside step function and sign function, respectively.

II. MODEL, ANDREEV BOUND STATES AND CONTINUUM DENSITY OF STATES

We consider a short QSHI-based topological JJ [56–58] employing the established δ -function model developed in Ref. [57] [for the geometry and configuration see Fig. 1, where for the most part of the paper we focus on the setup with a single proximitized edge as shown in Fig. 1(a)]. We assume the Fermi level is tuned to the bulk gap of the QSHI. Hence, the only propagating modes are the spin-polarized edge states. When the width \mathcal{W}_S of the junction is wide enough—as assumed in this paper—the QSHI edge states (referred to as the top and

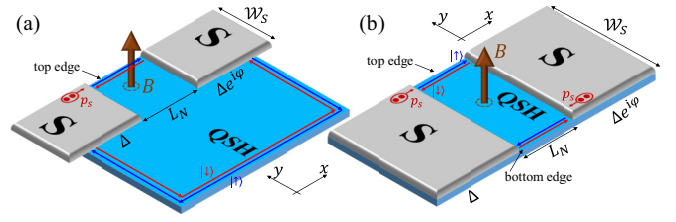


FIG. 1. Topological Josephson junctions formed by (a) one and (b) two QSHI edges. Here the QSHI is partially covered by two s -wave superconductors with different superconducting phases, the Cooper-pair tunneling induces superconducting proximity pairings in the corresponding regions of the QSHI, defining the superconducting (S) and normal (N) spacers. The N region is subtended by a perpendicular magnetic field \mathbf{B} . The coordinate system is chosen in such a way that the QSHI lies in the xy plane, with x being the transport direction defined by the gradient of the superconducting phase, correspondingly, $\mathbf{B} = B\mathbf{e}_z$. The edge with a positive (negative) ordinate y is called the top (bottom).

bottom edges/channels) do not overlap and their low-energy dynamics decouple. Correspondingly, the physics at each edge can be accurately described by the Bogoliubov-de Gennes (BdG) Hamiltonian,

$$\hat{H}_s^\sigma = (s\sigma v_F \hat{p}_x - \mu_S)\tau_z + s \frac{v_F P_S}{2} + V_0 h(x)\tau_z + \Delta[\tau_x \cos \Phi^\sigma(x) - \tau_y \sin \Phi^\sigma(x)]. \quad (1)$$

In the above equation, $\hat{p}_x = -i\hbar\partial_x$ denotes the momentum operator, μ_S represents the chemical potential in the superconducting (S) regions, V_0 is the potential difference between the normal (N) and S regions, and the (super/sub)scripts $s = \uparrow/\downarrow \equiv \pm 1$ and $\sigma = t/b \equiv \pm 1$ represent the spin projections along the z axis and the top and bottom channels, respectively. Finally, $\tau_{x,y,z}$ are Pauli matrices operating on the particle-hole degrees of freedom. We consider junctions where the top and bottom edge states have the same Fermi velocity ($v_F = v_F^{t/b}$), although junctions with $v_F^t \neq v_F^b$ are also possible, as discussed in Sec. VI. We limit our study to short junctions, where the length of the N region L_N is shorter than the superconductor coherence length. Furthermore, we also assume L_N to be shorter than the Josephson penetration depth, such that Josephson vortices and Fraunhofer features do not affect the system under consideration. Therefore, the N region can be effectively modeled as a δ -like spacer with a potential profile $h(x) = L_N\delta(x)$. The QSHI is proximitized by two s -wave superconductors which are assumed to have equal gap magnitudes, but different superconducting phases. Consequently, the induced superconducting pairing in the QSHI, $\Delta e^{i\phi(x)}$, retains a constant gap amplitude Δ , but an x -dependent phase $\phi(x)$, $\phi(x < 0) = 0$ and $\phi(x > 0) = \phi$, resulting in a global phase difference ϕ . An out-of-plane magnetic field $\mathbf{B} = B\mathbf{e}_z$ with $B \geq 0$ induces [58] (i) an orbital Doppler shift described by the Cooper pair momentum p_S and (ii) the edge-selective superconducting-phase profiles $\Phi^\sigma(x)$ with $\Phi^\sigma(x < 0) = 0$ and $\Phi^\sigma(x > 0) = \phi^\sigma$, where

$$p_S = \pi\hbar \frac{B\mathcal{W}_S}{\Phi_0}, \quad \phi^\sigma = \phi + \sigma \frac{p_S L_N}{\hbar}. \quad (2)$$

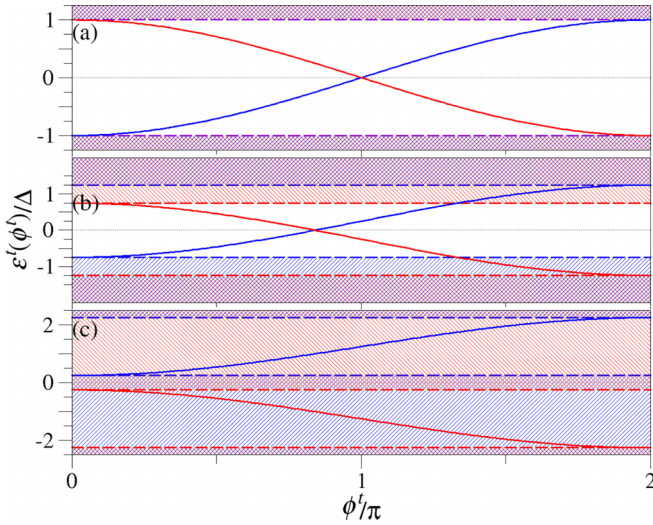


FIG. 2. ABS given by Eq. (3) for the top edge for different values of the dimensionless parameter $\gamma = v_F p_S / (2\Delta)$ [defined below in Eq. (10)]: (a) $\gamma = 0$, (b) $\gamma = 0.25$, (c) $\gamma = 1.25$. Here the blue and red colors denote different spin quantum numbers $s = \uparrow/\downarrow \equiv \pm 1$ associated with the subgap ABS (solid lines) and the supragap continuum states (shadings).

The second term in ϕ^σ can be interpreted as a kinematic phase acquired by a Cooper pair with a momentum σp_S when traversing a distance of L_N .

Following Refs. [57,59], the ABS spectra associated with the model Hamiltonian, Eq. (1), are determined by means of the spectral scattering approach, which yields per each edge (indexed by σ) two ABS branches (indexed by spin s) with an obvious 2π periodicity,

$$\epsilon_s^\sigma(\phi^\sigma) = s \left[-\sigma \Delta \cos \frac{\phi^\sigma}{2} \operatorname{sgn} \left(\sin \frac{\phi^\sigma}{2} \right) + \frac{v_F p_S}{2} \right]. \quad (3)$$

When $\phi^\sigma = \phi^{t/b}$ approaches an integer multiple of 2π , a pair of the subgap ABS with opposite spin projections merges into the continuum of quasiparticle states, see Fig. 2, while a pair of ABS with the reversed spins splits-off from the supragap states.

Complementary, the continuum of quasi-particles contributes to the supra-gap density of states (DOS) that can be separated into a phase-independent (shown explicitly later) and phase-dependent part. It is the latter, which is important for the computation of the Josephson current via differentiation of the free energy with respect to the superconducting phase difference. The phase-dependent part of the DOS, per spin and edge, can be compactly written as

$$\rho_s^\sigma(\epsilon, \phi^\sigma) = \frac{s\sigma \Delta^2}{2\pi} \frac{\Theta(\epsilon_s^2 - \Delta^2) \operatorname{sgn}(\epsilon_s) \sin \phi^\sigma}{\sqrt{\epsilon_s^2 - \Delta^2} (\epsilon_s^2 - \Delta^2 \cos^2 \frac{\phi^\sigma}{2})} \quad (4)$$

with

$$\epsilon_s = \epsilon - s v_F p_S / 2. \quad (5)$$

Although $\rho_s^\sigma(\epsilon, \phi^\sigma)$ can be negative, the total DOS, which also includes the phase-independent part, is always positive. As discussed in Ref. [57], a finite $v_F p_S$ decreases the effective superconducting gap, which closes for $|v_F p_S| \geq 2\Delta$.

However, for each spin species saddled by the opposite edges of the QSHI the superconducting gaps still remain open individually, and although energetically not overlapping, see Fig. 2(c), the bound and continuum states exist simultaneously on a spatial scale defined by the junction width \mathcal{W}_S . In the following, we will focus mainly on the setup with only one proximitized edge, as shown in Fig. 1(a).

III. FREE ENERGY AND CURRENT

The ABS spectra, Eq. (3), and the supragap DOS due to continuum states, Eq. (4), allow us to determine the free energy from which the Josephson current and other thermodynamic quantities follow straightforwardly. As the edges of the QSHI-based JJ are dynamically decoupled, the total free energy turns into a sum of its top and bottom parts. Hence, in an equilibrium held at temperature T and magnetic field $B \geq 0$, the free energy $F^\sigma(\phi^\sigma, T)$ of the edge σ (more precisely its phase-dependent part) equals

$$F^\sigma(\phi^\sigma, T) = -k_B T \left\{ \ln \left[2 \cosh \left(\frac{\epsilon_\uparrow^\sigma(\phi^\sigma)}{2k_B T} \right) \right] + \int_0^\infty d\epsilon \rho^\sigma(\epsilon, \phi^\sigma) \ln \left[2 \cosh \left(\frac{\epsilon}{2k_B T} \right) \right] \right\}. \quad (6)$$

Equation (6) consists of a discrete part due to ABS and of a continuum part, which integrates over the supragap DOS summed over both spin projections,

$$\rho^\sigma(\epsilon, \phi^\sigma) = \sum_{s=\uparrow/\downarrow} \rho_s^\sigma(\epsilon, \phi^\sigma). \quad (7)$$

As the superconducting phase difference ϕ and the edge-saddled phase difference ϕ^σ differ by just a shift, Eq. (2), the Josephson current carried by an edge σ is then calculated as

$$I^\sigma(\phi^\sigma, T) = \frac{2e}{\hbar} \frac{\partial F^\sigma(\phi^\sigma, T)}{\partial \phi^\sigma} = \frac{2e}{\hbar} \frac{\partial F^\sigma(\phi^\sigma, T)}{\partial \phi}. \quad (8)$$

Inserting Eqs. (3) and (4) into the free energy $F^\sigma(\phi^\sigma, T)$, the Josephson current splits into ABS and continuum contributions,

$$I^\sigma(\phi^\sigma, T) = I_{\text{ABS}}^\sigma(\phi^\sigma, T) + I_{\text{cont}}^\sigma(\phi^\sigma, T). \quad (9)$$

Introducing the short-hand notations,

$$I_0 = \frac{e\Delta}{2\hbar}, \quad \gamma = \frac{v_F p_S}{2\Delta}, \quad \tilde{\Delta} = \frac{\Delta}{2k_B T}, \quad (10)$$

the current contributions read,

$$I_{\text{ABS}}^\sigma(\phi^\sigma, T) = I_0 \sin \frac{\phi^\sigma}{2} \tanh \left[\tilde{\Delta} \left(\cos \frac{\phi^\sigma}{2} - \sigma \gamma \operatorname{sgn} \left(\sin \frac{\phi^\sigma}{2} \right) \right) \right] \quad (11)$$

and

$$I_{\text{cont}}^\sigma(\phi^\sigma, T) = -I_0 \frac{\sigma}{\tilde{\Delta}} \frac{1}{\pi} \int_1^\infty dx \ln \left[\frac{\cosh(\tilde{\Delta}(x + \gamma))}{\cosh(\tilde{\Delta}(x - \gamma))} \right] \times \frac{x^2 \cos \phi^\sigma - \cos^2 \frac{\phi^\sigma}{2}}{\sqrt{x^2 - 1} (x^2 - \cos^2 \frac{\phi^\sigma}{2})^2}. \quad (12)$$

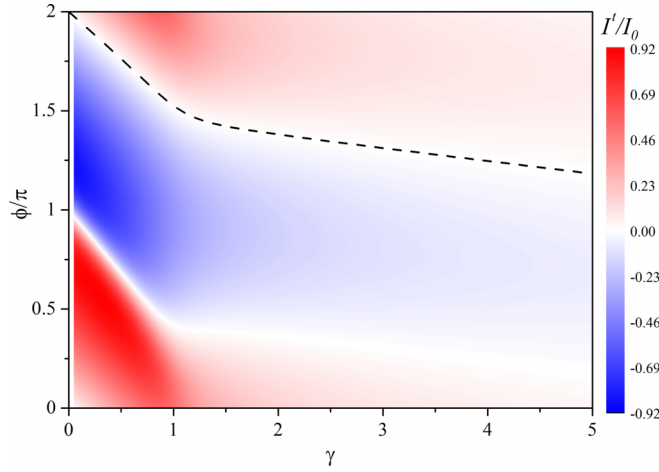


FIG. 3. Josephson current I' , composed of the ABS and continuum states, carried by the top edge of the QSHI-based junction plotted as a function of the phase difference ϕ and parameter $\gamma = v_F p_S / (2\Delta) \propto B$. The dashed line traces the evolution of the superconducting phase difference ϕ that minimizes the top-edge free energy at a given value of γ . Here $k_B T = 0.1\Delta$, $L_N \Delta / \hbar v_F = 0.1$, and the current I' is measured in units of $I_0 = e\Delta / (2\hbar)$.

At zero magnetic field, γ reduces to zero and consequently Eq. (12) gives no contribution, which is consistent with the expectation that in field-free short junctions the supercurrent is driven by the sub-gap states.

Figure 3 shows the top-edge current-phase relation, $I'(\phi)$, normalized to I_0 at $k_B T = 0.1\Delta$ as a function of the phase difference ϕ and the dimensionless parameter $\gamma \propto B$ [see Eq. (10)]. As γ increases, the maxima (red loci), minima (blue loci), and zeros (white trench) of the current-phase relation move along the ϕ axis, while, simultaneously, the amplitude of the Josephson current reduces.

It follows from Eq. (8) that the points (γ, ϕ^t) where I' vanishes and the free energy F^t minimizes—shown in Fig. 3 by the black dashed line—determine the ground-state phase, i.e., the phase at which the top edge is in its ground state for a given γ (magnetic field). As shown in Fig. 3, increasing γ causes the ground-state phase to shift from 2π (~ 0) to π , resulting in the top junction edge undergoing a $0 - \pi$ -like transition. The second white trench seen in Fig. 3, emanating from $\phi = \pi$ at $\gamma = 0$, corresponds to maxima of the free energy F^t . The supercurrent at the bottom edge can readily be obtained from Fig. 3 by using the symmetry relation $I^b(\phi, \gamma) = -I^t(2\pi - \phi, \gamma)$.

In the low-temperature limit, the integration in Eq. (12) can be performed analytically and the contribution from the continuum of states at the top/bottom edge reduces to

$$I_{\text{cont}}^{\sigma}(\phi^{\sigma}, T \rightarrow 0) = \sigma \frac{2I_0}{\pi} \left\{ \gamma + \Theta(\gamma - 1) \left[\arctan \left(\frac{\sqrt{\gamma^2 - 1}}{\sin \frac{\phi^{\sigma}}{2}} \right) \times \sin \frac{\phi^{\sigma}}{2} - \sqrt{\gamma^2 - 1} \right] \right\}. \quad (13)$$

Note that the above equation has been derived assuming $B \geq 0$ or equivalently $\gamma \geq 0$. To obtain the corresponding expression for $B < 0$, the relation $I^{\sigma}(B, \phi) = I^{-\sigma}(-B, \phi)$

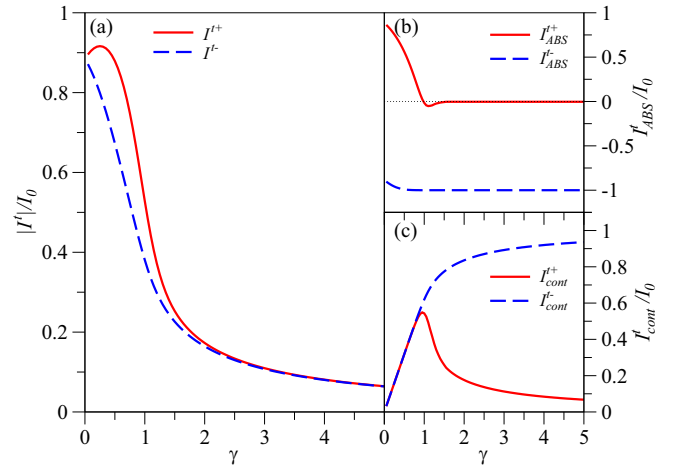


FIG. 4. Top edge Josephson current characteristics for a QSHI-based JJ. Panel (a) displays maximal (red), I'^{+} , and minimal (blue), I'^{-} , critical currents (normalized to I_0) as functions of $\gamma = v_F p_S / (2\Delta) \propto B$. Panels (b) and (c) show, correspondingly, the ABS contribution, I_{ABS}^{\pm} , and continuum-state contribution, I_{cont}^{\pm} , of I'^{\pm} . Again the maxima and minima are plotted in red and blue.

can be used. It is instructive to connect the dependence of $I_{\text{cont}}^{\sigma}(\phi^{\sigma}, T \rightarrow 0)$ on γ with the closing of the effective superconducting gap, see Fig. 2(b), and of the lifting of the protected ABS crossing, see Fig. 2(c), when $\gamma = v_F p_S / (2\Delta)$ exceeds unity.

IV. SUPERCONDUCTING DIODE EFFECT AND Q FACTOR

The maximum $I^{\sigma+} = \max_{\phi^{\sigma}} I^{\sigma}(\phi^{\sigma})$ and minimum $I^{\sigma-} = \min_{\phi^{\sigma}} I^{\sigma}(\phi^{\sigma})$ of the total Josephson current for a given edge, σ , at a given magnetic field $B \propto \gamma$ determine the Q factor, $Q^{\sigma}(\gamma, T)$. The latter serves as a figure of merit quantifying the SDE as a function of the out-of-plane field and temperature,

$$Q^{\sigma}(\gamma, T) = \frac{|I^{\sigma+}| - |I^{\sigma-}|}{I_0}. \quad (14)$$

Combining the low-temperature limit of Eq. (11) with Eq. (13) yields

$$Q^{\sigma}(\gamma, T \rightarrow 0) = \sigma \left\{ \left(\sqrt{1 - \gamma^2} - 1 + \frac{4\gamma}{\pi} \right) \Theta(1 - \gamma) + \left[\frac{4}{\pi} (\gamma - \sqrt{\gamma^2 - 1}) + \frac{2}{\pi} \arctan(\sqrt{\gamma^2 - 1}) - 1 \right] \Theta(\gamma - 1) \right\}. \quad (15)$$

Figure 4 illustrates the behavior of the Josephson current on the top edge. In particular, the maximal and minimal Josephson currents, I'^{+} and I'^{-} , are displayed in Fig. 4(a) as functions of $\gamma \propto B$, while different contributions to I'^{\pm} , carried by the ABS and continuum states, are plotted in Figs. 4(b) and 4(c). As already observed in Fig. 3, the Josephson current gets suppressed with increasing γ , and thus also $I^{\sigma\pm}$. Con-

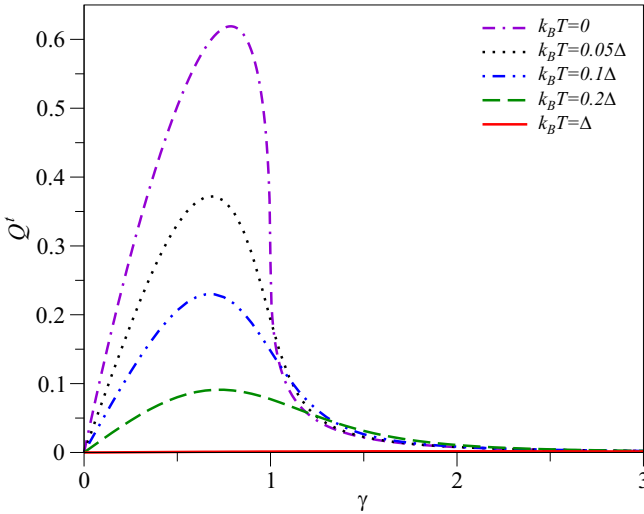


FIG. 5. Diode effect Q factor, Eq. (14), for the top edge of a QSHI-based JJ as a function of $\gamma \propto B$ displayed for different temperatures. Here $Q^t(T \rightarrow 0)$ is computed by means of Eq. (15).

sequently, the Q factor is expected to approach zero when γ increases.

This is borne out by Fig. 5, which shows the Q factor of the top edge for different temperatures. According to Eq. (15), the Q factor at $T = 0$ exhibits a pronounced

maximum $Q_{\max}^t = \sqrt{16/\pi^2 + 1} - 1 \approx 0.618993$ at $\gamma_{\max} = 1/\sqrt{1 + \pi^2/16} \approx 0.786439$. The fact that both Q_{\max}^t and γ_{\max} reduce to universal values, independent of junction parameters, is quite remarkable [60]. As T increases, the Q factor decreases until the pronounced peak observed at low temperatures is no longer discernible [see, for example, the solid line corresponding to $k_B T = \Delta$ in Fig. 5].

It is clear from Eq. (15) that the net Q factor of the narrow topological JJs, consisting of top and bottom edges, $Q_{\text{tot}} = Q^t + Q^b$, vanishes because $Q^t = -Q^b$ (see also Appendix B). Hence, to realize a finite SDE in QSHI-based junctions, a setup with disparate QSHI edges is required. This can be achieved, for example, by using the setup depicted in Fig. 1(a), where the superconductor proximitizes only one edge (the top edge in this case), or by designing the heterojunction in a way that the corresponding Fermi velocities v_F^t and v_F^b become substantially different.

V. PARITY CONSERVING SUPERCONDUCTING DIODE EFFECT

Having discussed the SDE in a situation without constraints on the fermion parity, we now discuss a scenario in which the fermionic ground-state parity is conserved. To keep track of that, all underlying quantities are indexed by the subscript p . Correspondingly, the parity-conserved free energy—up to phase-independent contributions—reads [57,61,62]

$$F_p^\sigma(\phi^\sigma, T) = F^\sigma(\phi^\sigma, T) - k_B T \ln \left\{ \frac{1}{2} \left[1 + p P_\sigma(\phi^\sigma) \tanh \left| \frac{\epsilon_\uparrow^\sigma(\phi^\sigma)}{2k_B T} \right| \right] \exp \left[J_S(T) + \int_0^\infty d\epsilon \rho_{\text{tot}}^\sigma(\epsilon, \phi^\sigma) \ln \left[\tanh \left(\frac{\epsilon}{2k_B T} \right) \right] \right] \right\}, \quad (16)$$

where the equilibrium free energy $F^\sigma(\phi^\sigma, T)$ is given by Eq. (6) and the parity factor equals

$$P_\sigma(\phi^\sigma) = \text{sgn} \left[\cos \frac{\phi^\sigma}{2} - \sigma \gamma \text{sgn} \left(\sin \frac{\phi^\sigma}{2} \right) \right]. \quad (17)$$

The above form of $P_\sigma(\phi^\sigma)$ implies a convention according to which the fermionic parity $p = +1$ corresponds to the lower, and $p = -1$ to the upper spectral branches in Fig. 2, where lower and upper refer to energies near $\phi = 0$.

In contrast to the Josephson current $I^\sigma(\phi^\sigma, T)$ derived from the equilibrium free energy $F^\sigma(\phi^\sigma, T)$, the parity conserving Josephson current $I_p^\sigma(\phi^\sigma, T)$ derived from $F_p^\sigma(\phi^\sigma, T)$ via Eq. (8), involves the total quasiparticle DOS, $\rho_{\text{tot}}^\sigma(\epsilon, \phi^\sigma) = \rho_\sigma(\epsilon, \phi^\sigma) + \bar{\rho}_0(\epsilon)$, which, in addition to the term $\rho^\sigma(\epsilon, \phi^\sigma)$ given by Eq. (7), contains the phase-independent contribution,

$$\bar{\rho}_0(\epsilon) = \frac{2}{\pi E_S} \sum_{s=\uparrow/\downarrow} |\epsilon_s| \frac{\Theta(\epsilon_s^2 - \Delta^2)}{\sqrt{\epsilon_s^2 - \Delta^2}}, \quad (18)$$

where the energy scale, $E_S = \hbar v_F / L_S$, is related to the total length L_S of the superconducting QSHI edge. In a similar way, the ϕ -independent DOS of the superconducting electrodes on top of the QSHI contribute with [63]

$$J_S(T) = -\frac{2}{\pi k_B T E_S} \int_\Delta^\infty d\epsilon \frac{\sqrt{\epsilon^2 - \Delta^2}}{\sinh(\epsilon/k_B T)}. \quad (19)$$

Although the underlying expressions get more involved when compared to Secs. III and IV, still some approximate analytical results can be obtained in the limiting case $T \rightarrow 0$ and $\gamma \ll 1$. However, one needs to pay attention in which order are the corresponding mathematical operations taken into action: first goes an integration in Eq. (16), then a derivative with respect to ϕ , and finally the limit $T \rightarrow 0$. Proceeding in this way, the current for a fixed fermionic parity $p = \pm 1$ reduces to

$$I_p^\sigma(\phi^\sigma, T \rightarrow 0) = \sigma I_0 \left(p \sin \frac{\phi^\sigma}{2} + \frac{2\gamma}{\pi} \right), \quad \gamma \ll 1 \quad (20)$$

with the corresponding Q factor [see Eq. (14)]

$$Q_p^\sigma(\gamma, T \rightarrow 0) = \sigma \frac{4\gamma}{\pi}, \quad \gamma \ll 1. \quad (21)$$

While Eqs. (20) and (21) already provide some useful guidance, we proceed fully numerically for a more detailed analysis.

Figure 6 shows the parity conserving Josephson currents, $I_{p=\pm 1}^\sigma(\phi^\sigma, T)$, at the top edge, for both fermionic parities $p = \pm 1$. In contrast to the parity unconstrained Josephson current, $I^\sigma(\phi^\sigma, T)$, which exhibits 2π periodicity, its parity-conserved counterpart, c , becomes 4π periodic [57,61,62]. Intriguingly, Fig. 6 illustrates that the current-phase relations of the two different parities $p = \pm 1$ are only shifted along the ϕ axis with

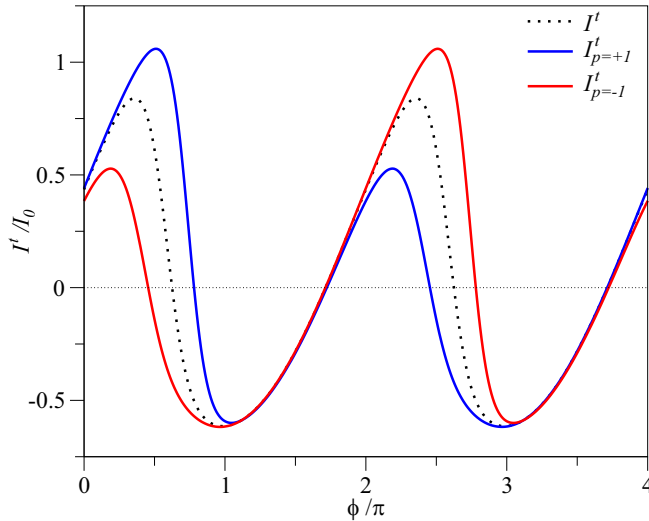


FIG. 6. Josephson current carried by the top edge of a QSHI-based JJ plotted as a function of the phase difference ϕ with (solid lines) and without (dashed line) parity constraints: I^t stands for parity unconstrained 2π periodic current, Secs. II–IV, while $I_{p=\pm 1}^t$ denotes parity conserved 4π periodic currents with $p = \pm 1$. Here $\gamma = 0.6$, $k_B T = 0.1\Delta$, $E_S = 0.05\Delta$, $L_N \Delta / \hbar v_F = 0.1$, and the currents are measured in units of $I_0 = e\Delta / (2\hbar)$.

respect to each other, implying the Q factor to be independent of the value of p , as also shown by Eq. (21). Moreover, one can discern from Fig. 6 that for $\gamma < 1$ the asymmetry between the magnitudes of the maximal and minimal values of the Josephson current increases when the fermionic ground-state parity is kept conserved. This, in turn, implies that for $\gamma < 1$ parity conservation enhances the SDE, as evidenced by Fig. 7, where the magnetic-field dependence of the Q factor [see Eq. (14)] is shown for $p = +1$ and various temperatures. Indeed, by comparing Figs. 5 and 7 we can observe that, at a given temperature, the parity-conserved Q factor

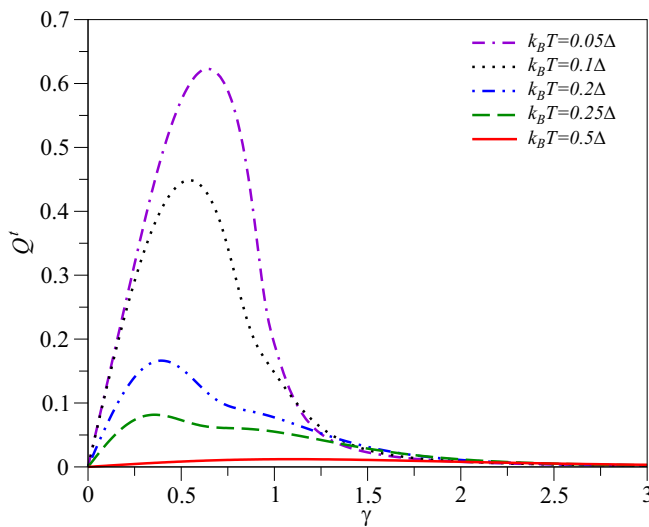


FIG. 7. Diode effect Q factor, Eq. (14), for the top edge of QSHI-based JJ with the parity $p = +1$ as a function of $\gamma \propto B$ and different temperatures. Here $E_S = 0.05\Delta$. Note that the Q factor for $p = -1$ is the same as that for $p = +1$.

is generally larger than its parity-unconstrained counterpart, as long as the magnetic field keeps the global superconducting gap open (that is, when $\gamma < 1$). The parity-enhanced Q factor is reminiscent of the enhanced parity-protected SDE predicted in semiconductor-based Majorana wires [26]. However, when $\gamma \geq 1$, the additional contributions in Eq. (16) tend to zero and $F_p^\sigma(\phi^\sigma, T)$ tends to the equilibrium free energy $F^\sigma(\phi^\sigma, T)$. Therefore, the Q factors for the case with and without fermionic parity conservation approach each other when $\gamma \geq 1$. For low temperatures, Q increases linearly (see Fig. 7), which is perfectly described by Eq. (21).

While we predict that for magnetic fields such that $\gamma < 1$, topological JJs with conserved fermionic parity exhibit larger Q factors than their parity unconstrained counterparts, their experimental realization becomes more challenging, as will be discussed in the following section.

VI. EXPERIMENTAL REALIZATIONS

Turning to potential experimental realizations displaying the SDE, we first consider the situation, where the fermionic ground-state parity does not play a role. As discussed above, if both edges of the QSHI-based JJ are equivalent [e.g., as illustrated in Fig. 1(b)], their contributions to the SDE cancel each other out. One way to overcome this difficulty is to design the system so that the two edges of the JJ become nonequivalent. For example, by predominantly transporting Cooper pairs along one edge, as shown in Fig. 1(a). In this configuration, only the top edge constitutes a short JJ, while the bottom edge forms a long JJ that carries less current due to a diminished contribution from the ABS. Consequently, the Q factor is dominated by that of the top edge, making the single-edge physics discussed in Sec. IV experimentally relevant.

Another way to make the edges nonequivalent is by endowing them with different Fermi velocities. For instance, in $\text{Hg}_{1-x}\text{Cd}_x\text{Te}/\text{HgTe}/\text{Hg}_{1-x}\text{Cd}_x\text{Te}$ -based quantum wells realizing a QSHI, the bandgap and Fermi velocity depend on (i) the thickness of the HgTe spacer [64,65] and (ii) the stoichiometric ratio of the Cd compound [66,67]. Therefore, manufacturing HgTe-based quantum wells with different thicknesses and/or different Cd concentrations at opposite edges will make the edges nonequivalent, resulting in an observable nonzero SDE. For such HgTe-based junctions, thin-film aluminium has been used successfully to induce superconductivity in the presence of magnetic fields of more than 1 T in the normal region [68,69]. We expect much smaller magnetic fields, well below the critical magnetic field of the parent superconductor, are needed to observe a sizable SDE in such a system, however [70].

While we anticipate a finite SDE for QSHI junctions with a single edge or nonequivalent edges in a situation without parity constraints, preserving the fermionic parity of the ground state in experimental setups poses additional challenges, requiring conducting experiments on timescales shorter than the quasiparticle poisoning rate [71,72]. For the topological JJs based on $\text{Hg}_{1-x}\text{Cd}_x\text{Te}/\text{HgTe}/\text{Hg}_{1-x}\text{Cd}_x\text{Te}$, such timescales become of the order of $1 \mu\text{s}$ [73–75]. Consequently, experiments aiming to measure the parity-conserving SDE must operate within a sub- μs range. Nevertheless, with modern qubit and SQUID technologies enabling controlled modula-

tion of ϕ on timescales of 1 ns or shorter [76], the observation of a parity-conserving SDE in narrow topological JJs, despite being challenging, should be experimentally feasible.

VII. CONCLUSIONS

In this work we have studied the SDE in narrow topological QSHI-based JJs triggered by an out-of-plane magnetic field. In general, the realization of the SDE in QSHI-based JJs requires the transport of Cooper pairs through nonequivalent edge channels at the opposite ends of the junction. We investigated two different parity regimes—the conventional, so-called parity-unconstrained regime and a novel one, where the fermionic parity of the ground state is preserved. Our findings demonstrate that QSHI-based JJs can be used as versatile experimental platforms showcasing the SDE. Furthermore, our calculations predict an increase in the Q factor and, consequently, the diode efficiency as the temperature decreases. Interestingly, in the parity-unconstrained low-temperature regime, the maximum diode efficiency exhibits a universal character, with the maximum Q -factor value being independent of the system and Hamiltonian parameters. This remarkable behavior appears to be a direct consequence of the topological nature of edge-state charge transport in the QSHI regime.

Complementary to detailed numerical simulations, we also provide valuable analytical results that can be readily applied to understanding, interpreting, and fitting experimental data.

ACKNOWLEDGMENTS

D.K. acknowledges partial support from Project IM-2021-26 (SUPERSPIN) funded by the Slovak Academy of Sciences via the programme IMPULZ 2021, and VEGA Grant No. 2/0156/22—QuaSiModo. A.M.A. acknowledges support from ONR Grant No. N000141712793.

APPENDIX A: ALTERNATIVE DEFINITION OF Q FACTOR

In addition to the definition of the Q factor as given in Eq. (14), one can alternatively define the Q factor as

$$Q_{\text{alt}}^{\sigma}(\gamma, T) = \frac{|I^{\sigma+}| - |I^{\sigma-}|}{|I^{\sigma+}| + |I^{\sigma-}|}, \quad (\text{A1})$$

where $I^{\sigma+}$ and $I^{\sigma-}$ are the global maxima and minima of the Josephson current, respectively. The dependence of $Q_{\text{alt}}^{\sigma}(\gamma, T)$ on γ is shown in Fig. 8 for different values of the temperature. In the zero-temperature limit the Q factor defined by Eq. (A1) can be written as

$$\begin{aligned} Q_{\text{alt}}^{\sigma}(\gamma, T \rightarrow 0) &= \sigma \left\{ \frac{\sqrt{1-\gamma^2} - 1 + 4\gamma/\pi}{\sqrt{1-\gamma^2} + 1} \Theta(1-\gamma) \right. \\ &\quad \left. + \left[\frac{2(\gamma - \sqrt{\gamma^2 - 1})}{\pi/2 - \arctan(\sqrt{\gamma^2 - 1})} - 1 \right] \Theta(\gamma - 1) \right\}. \quad (\text{A2}) \end{aligned}$$

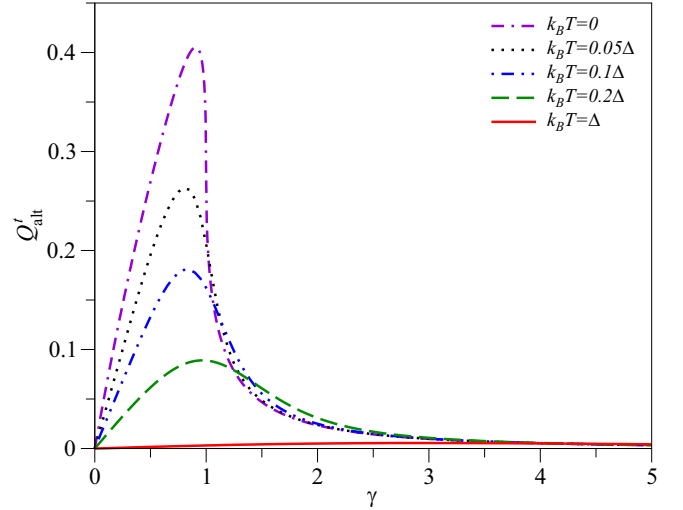


FIG. 8. Q factor of the top edge, Q'_{alt} , see Eq. (A1), as a function of $\gamma = v_F p_S / (2\Delta) \propto B$ for different temperatures. $Q(T \rightarrow 0)$ is computed from Eq. (A2).

APPENDIX B: JOSEPHSON CURRENT AT THE TOP AND BOTTOM EDGES

As discussed in the main text, if the edge states at the opposite ends (say, top and bottom) of the QSHI-based JJ are equivalent, the SDE contribution at the top and bottom edges cancel each other out, leading to a vanishing Q factor. This is illustrated in Fig. 9, where the total Josephson current, $I_{\text{tot}}(\phi, T) = I^t(\phi, T) + I^b(\phi, T)$, as well as the individual contributions from the top and bottom edges are shown. When the edges are equivalent, their associated currents $I^t(\phi, T)$ and $I^b(\phi, T)$ obey the symmetry relation, $\max[I_{\text{tot}}(\phi, T)] = |\min[I_{\text{tot}}(\phi, T)]|$, which in turn implies that $Q_{\text{tot}} = 0$.

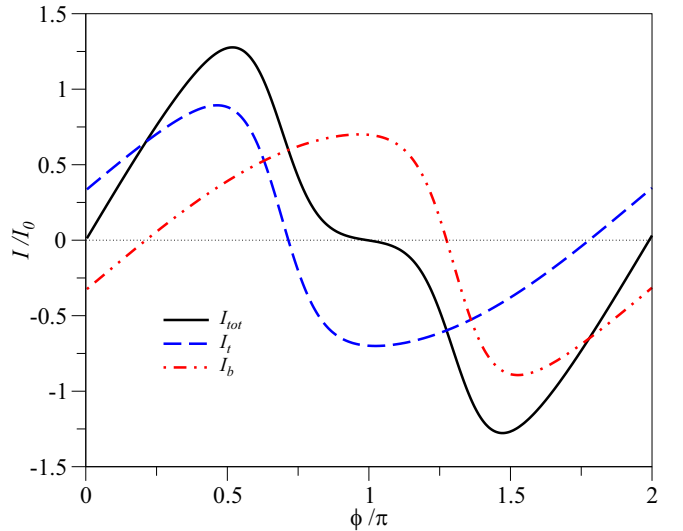


FIG. 9. Total Josephson current (black) of a QSHI-based JJ and the individual contributions from the top (blue) and bottom (red) edges as a function of the phase difference ϕ . Here $v_F p_S = 0.9\Delta$ and $L_N \Delta / \hbar v_F = 0.1$.

- [1] M. Nadeem, M. S. Fuhrer, and X. Wang, The superconducting diode effect, *Nat. Rev. Phys.* **5**, 558 (2023).
- [2] A. G. Sivakov, O. G. Turutanov, A. E. Kolinko, and A. S. Pokhila, Spatial characterization of the edge barrier in wide superconducting films, *Low Temp. Phys.* **44**, 226 (2018).
- [3] D. Y. Vodolazov, A. Y. Aladyshkin, E. E. Pestov, S. N. Vdovichev, S. S. Ustavshikov, M. Y. Levichev, A. V. Putilov, P. A. Yunin, A. I. El'kina, N. N. Bukharov, and A. M. Klushin, Peculiar superconducting properties of a thin film superconductor–normal metal bilayer with large ratio of resistivities, *Supercond. Sci. Technol.* **31**, 115004 (2018).
- [4] F. Ando, Y. Miyasaka, T. Li, J. Ishizuka, T. Arakawa, Y. Shiota, T. Moriyama, Y. Yanase, and T. Ono, Observation of superconducting diode effect, *Nature (London)* **584**, 373 (2020).
- [5] Y. Hou, F. Nichele, H. Chi, A. Lodesani, Y. Wu, M. F. Ritter, D. Z. Haxell, M. Davydova, S. Ilić, O. Glezakou-Elbert, A. Varambally, F. S. Bergeret, A. Kamra, L. Fu, P. A. Lee, and J. S. Moodera, Ubiquitous superconducting diode effect in superconductor thin films, *Phys. Rev. Lett.* **131**, 027001 (2023).
- [6] C. Baumgartner, L. Fuchs, A. Costa, S. Reinhardt, S. Gronin, G. C. Gardner, T. Lindemann, M. J. Manfra, P. E. Faria Junior, D. Kochan, J. Fabian, N. Paradiso, and C. Strunk, Supercurrent rectification and magnetochiral effects in symmetric Josephson junctions, *Nat. Nanotechnol.* **17**, 39 (2022).
- [7] C. Baumgartner, L. Fuchs, A. Costa, J. Picó-Cortés, S. Reinhardt, S. Gronin, G. C. Gardner, T. Lindemann, M. J. Manfra, P. E. F. Junior, D. Kochan, J. Fabian, N. Paradiso, and C. Strunk, Effect of Rashba and Dresselhaus spin-orbit coupling on supercurrent rectification and magnetochiral anisotropy of ballistic Josephson junctions, *J. Phys.: Condens. Matter* **34**, 154005 (2022).
- [8] B. Turini, S. Salimian, M. Carrega, A. Iorio, E. Strambini, F. Giazotto, V. Zannier, L. Sorba, and S. Heun, Josephson diode effect in high-mobility insb nanoflags, *Nano Lett.* **22**, 8502 (2022).
- [9] A. Costa, C. Baumgartner, S. Reinhardt, J. Berger, S. Gronin, G. C. Gardner, T. Lindemann, M. J. Manfra, J. Fabian, D. Kochan, N. Paradiso, and C. Strunk, Sign reversal of the Josephson inductance magnetochiral anisotropy and $0-\pi$ -like transitions in supercurrent diodes, *Nat. Nanotechnol.* **18**, 1266 (2023).
- [10] N. Lotfizadeh, W. F. Schiela, B. Pekerten, P. Yu, B. H. Elfeky, W. M. Strickland, A. Matos-Abiague, and J. Shabani, Superconducting diode effect sign change in epitaxial al-inas Josephson junctions, *Commun. Phys.* **7**, 120 (2024).
- [11] S. Reinhardt, T. Ascherl, A. Costa, J. Berger, S. Gronin, G. C. Gardner, T. Lindemann, M. J. Manfra, J. Fabian, D. Kochan, C. Strunk, and N. Paradiso, Link between supercurrent diode and anomalous Josephson effect revealed by gate-controlled interferometry, *Nat. Commun.* **15**, 4413 (2024).
- [12] B. Pal, A. Chakraborty, P. K. Sivakumar, M. Davydova, A. K. Gopi, A. K. Pandeya, J. A. Krieger, Y. Zhang, M. Date, S. Ju, N. Yuan, N. B. M. Schröter, L. Fu, and S. S. P. Parkin, Josephson diode effect from Cooper pair momentum in a topological semimetal, *Nat. Phys.* **18**, 1228 (2022).
- [13] K.-R. Jeon, J.-K. Kim, J. Yoon, J.-C. Jeon, H. Han, A. Cottet, T. Kontos, and S. S. P. Parkin, Zero-field polarity-reversible Josephson supercurrent diodes enabled by a proximity-magnetized Pt barrier, *Nat. Mater.* **21**, 1008 (2022).
- [14] R. Wakatsuki, Y. Saito, S. Hoshino, Y. M. Itahashi, T. Ideue, M. Ezawa, Y. Iwasa, and N. Nagaosa, Nonreciprocal charge transport in noncentrosymmetric superconductors, *Sci. Adv.* **3**, e1602390 (2017).
- [15] H. Wu, Y. Wang, Y. Xu, P. K. Sivakumar, C. Pasco, U. Filippozzi, S. S. P. Parkin, Y.-J. Zeng, T. McQueen, and M. N. Ali, The field-free Josephson diode in a van der Waals heterostructure, *Nature (London)* **604**, 653 (2022).
- [16] L. Bauriedl, C. Bäuml, L. Fuchs, C. Baumgartner, N. Paulik, J. M. Bauer, K.-Q. Lin, J. M. Lupton, T. Taniguchi, K. Watanabe, C. Strunk, and N. Paradiso, Supercurrent diode effect and magnetochiral anisotropy in few-layer NbSe₂, *Nat. Commun.* **13**, 4266 (2022).
- [17] J. Díez-Mérida, A. Díez-Carlón, S. Y. Yang, Y. M. Xie, X. J. Gao, J. Senior, K. Watanabe, T. Taniguchi, X. Lu, A. P. Higginbotham, K. T. Law, and D. K. Efetov, Symmetry-broken Josephson junctions and superconducting diodes in magic-angle twisted bilayer graphene, *Nat. Commun.* **14**, 2396 (2023).
- [18] J.-X. Lin, P. Siriviboon, H. D. Scammell, S. Liu, D. Rhodes, K. Watanabe, T. Taniguchi, J. Hone, M. S. Scheurer, and J. I. A. Li, Zero-field superconducting diode effect in small-twist-angle trilayer graphene, *Nat. Phys.* **18**, 1221 (2022).
- [19] S. Y. F. Zhao, X. Cui, P. A. Volkov, H. Yoo, S. Lee, J. A. Gardener, A. J. Akey, R. Engelke, Y. Ronen, R. Zhong, G. Gu, S. Plugge, T. Tummuru, M. Kim, M. Franz, J. H. Pixley, N. Poccia, and P. Kim, Time-reversal symmetry breaking superconductivity between twisted cuprate superconductors, *Science* **382**, 1422 (2023).
- [20] S. Ghosh, V. Patil, A. Basu, Kuldeep, A. Dutta, D. A. Jangade, R. Kulkarni, A. Thamizhavel, J. F. Steiner, F. von Oppen, and M. M. Deshmukh, High-temperature Josephson diode, *Nat. Mater.* **23**, 612 (2024).
- [21] S. Pal and C. Benjamin, Quantized Josephson phase battery, *Europhys. Lett.* **126**, 57002 (2019).
- [22] C.-Z. Chen, J. J. He, M. N. Ali, G.-H. Lee, K. C. Fong, and K. T. Law, Asymmetric Josephson effect in inversion symmetry breaking topological materials, *Phys. Rev. B* **98**, 075430 (2018).
- [23] Y. Tanaka, B. Lu, and N. Nagaosa, Theory of giant diode effect in d -wave superconductor junctions on the surface of a topological insulator, *Phys. Rev. B* **106**, 214524 (2022).
- [24] B. Lu, S. Ikegaya, P. Burset, Y. Tanaka, and N. Nagaosa, Tunable Josephson diode effect on the surface of topological insulators, *Phys. Rev. Lett.* **131**, 096001 (2023).
- [25] P.-H. Fu, Y. Xu, S. A. Yang, C. H. Lee, Y. S. Ang, and J.-F. Liu, Field-effect Josephson diode via asymmetric spin-momentum locking states, *Phys. Rev. Appl.* **21**, 054057 (2024).
- [26] H. F. Legg, K. Laubscher, D. Loss, and J. Klinovaja, Parity-protected superconducting diode effect in topological Josephson junctions, *Phys. Rev. B* **108**, 214520 (2023).
- [27] J. Cayao, N. Nagaosa, and Y. Tanaka, Enhancing the Josephson diode effect with Majorana bound states, *Phys. Rev. B* **109**, L081405 (2024).
- [28] J. S. Meyer and M. Houzet, Josephson diode effect in a ballistic single-channel nanowire, *Appl. Phys. Lett.* **125**, 022603 (2024).
- [29] D. Debnath and P. Dutta, Gate-tunable Josephson diode effect in Rashba spin-orbit coupled quantum dot junctions, *Phys. Rev. B* **109**, 174511 (2024).
- [30] M. Trahms, L. Melischek, J. F. Steiner, B. Mahendru, I. Tamir, N. Bogdanoff, O. Peters, G. Reecht, C. B. Winkelmann, F. von

- Oppen, and K. J. Franke, Diode effect in Josephson junctions with a single magnetic atom, *Nature (London)* **615**, 628 (2023).
- [31] S. Banerjee and M. S. Scheurer, Altermagnetic superconducting diode effect, *Phys. Rev. B* **110**, 024503 (2024).
- [32] S.-B. Zhang, L.-H. Hu, and T. Neupert, Finite-momentum cooper pairing in proximitized altermagnets, *Nat. Commun.* **15**, 1801 (2024).
- [33] M. Davydova, S. Prembabu, and L. Fu, Universal Josephson diode effect, *Sci. Adv.* **8**, eabo0309 (2022).
- [34] S. Fracassi, S. Traverso, N. Traverso Ziani, M. Carrega, S. Heun, and M. Sasseti, Anomalous supercurrent and diode effect in locally perturbed topological Josephson junctions, *Appl. Phys. Lett.* **124**, 242601 (2024).
- [35] M. Coraiola, A. E. Svetogorov, D. Z. Haxell, D. Sabonis, M. Hinderling, S. C. ten Kate, E. Cheah, F. Krizek, R. Schott, W. Wegscheider, J. C. Cuevas, W. Belzig, and F. Nichele, Flux-tunable Josephson diode effect in a hybrid four-terminal Josephson junction, *ACS Nano* **18**, 9221 (2024).
- [36] P.-H. Fu, J.-F. Liu, Y. Xu, C. H. Lee, and Y. Sin Ang, Transverse cooper-pair rectifier, [arXiv:2405.04751](https://arxiv.org/abs/2405.04751).
- [37] V. M. Edelstein, Characteristics of the Cooper pairing in two-dimensional noncentrosymmetric electron systems, *Sov. Phys. JETP* **68**, 1244 (1989).
- [38] V. M. Edelstein, The Ginzburg-Landau equation for superconductors of polar symmetry, *J. Phys.: Condens. Matter* **8**, 339 (1996).
- [39] A. Daido, Y. Ikeda, and Y. Yanase, Intrinsic superconducting diode effect, *Phys. Rev. Lett.* **128**, 037001 (2022).
- [40] N. F. Q. Yuan and L. Fu, Supercurrent diode effect and finite-momentum superconductors, *Proc. Natl. Acad. Sci. USA* **119**, e2119548119 (2022).
- [41] M. Smith, A. V. Andreev, and B. Z. Spivak, Giant magnetoconductivity in noncentrosymmetric superconductors, *Phys. Rev. B* **104**, L220504 (2021).
- [42] J. J. He, Y. Tanaka, and N. Nagaosa, A phenomenological theory of superconductor diodes, *New J. Phys.* **24**, 053014 (2022).
- [43] H. D. Scammell, J. I. A. Li, and M. S. Scheurer, Theory of zero-field superconducting diode effect in twisted trilayer graphene, *2D Mater.* **9**, 025027 (2022).
- [44] S. Ilić and F. S. Bergeret, Theory of the supercurrent diode effect in Rashba superconductors with arbitrary disorder, *Phys. Rev. Lett.* **128**, 177001 (2022).
- [45] T. de Picoli, Z. Blood, Y. Lyanda-Geller, and J. I. Väyrynen, Superconducting diode effect in quasi-one-dimensional systems, *Phys. Rev. B* **107**, 224518 (2023).
- [46] L. Fuchs, D. Kochan, J. Schmidt, N. Hüttner, C. Baumgartner, S. Reinhardt, S. Gronin, G. C. Gardner, T. Lindemann, M. J. Manfra, C. Strunk, and N. Paradiso, Anisotropic vortex squeezing in synthetic Rashba superconductors: A manifestation of Lifshitz invariants, *Phys. Rev. X* **12**, 041020 (2022).
- [47] A. Banerjee, M. Geier, M. A. Rahman, C. Thomas, T. Wang, M. J. Manfra, K. Flensberg, and C. M. Marcus, Phase asymmetry of Andreev spectra from cooper-pair momentum, *Phys. Rev. Lett.* **131**, 196301 (2023).
- [48] A. Sundaresh, J. I. Väyrynen, Y. Lyanda-Geller, and L. P. Rokhinson, Diamagnetic mechanism of critical current non-reciprocity in multilayered superconductors, *Nat. Commun.* **14**, 1628 (2023).
- [49] D. Kochan, A. Costa, I. Zhumagulov, and I. Žutić, Phenomenological theory of the supercurrent diode effect: The Lifshitz invariant, [arXiv:2303.11975](https://arxiv.org/abs/2303.11975).
- [50] A. Costa, J. Fabian, and D. Kochan, Microscopic study of the Josephson supercurrent diode effect in Josephson junctions based on two-dimensional electron gas, *Phys. Rev. B* **108**, 054522 (2023).
- [51] V. Mineev and K. Samokhin, Helical phases in superconductors, *JETP* **78**, 401 (1994).
- [52] O. Dimitrova and M. V. Feigel'man, Theory of a two-dimensional superconductor with broken inversion symmetry, *Phys. Rev. B* **76**, 014522 (2007).
- [53] A. Buzdin, Direct coupling between magnetism and superconducting current in the Josephson ϕ_0 Junction, *Phys. Rev. Lett.* **101**, 107005 (2008).
- [54] V. P. Mineev and M. Sigrist, Basic theory of superconductivity in metals without inversion center, in *Non-Centrosymmetric Superconductors*, edited by E. Bauer and M. Sigrist (Springer, Berlin, Heidelberg, 2012), pp. 129–154.
- [55] A. Costa, J. Fabian, and D. Kochan, Connection between zero-energy Yu-Shiba-Rusinov states and $0-\pi$ transitions in magnetic Josephson junctions, *Phys. Rev. B* **98**, 134511 (2018).
- [56] F. Dolcini, M. Houzet, and J. S. Meyer, Topological Josephson ϕ_0 junctions, *Phys. Rev. B* **92**, 035428 (2015).
- [57] B. Scharf, A. Braggio, E. Strambini, F. Giazotto, and E. M. Hankiewicz, Thermodynamics in topological Josephson junctions, *Phys. Rev. Res.* **3**, 033062 (2021).
- [58] G. Tkachov, P. Bursat, B. Trauzettel, and E. M. Hankiewicz, Quantum interference of edge supercurrents in a two-dimensional topological insulator, *Phys. Rev. B* **92**, 045408 (2015).
- [59] G. Tkachov, Chiral current-phase relation of topological Josephson junctions: A signature of the 4π -periodic Josephson effect, *Phys. Rev. B* **100**, 035403 (2019).
- [60] For the bottom edge, there is a minimum at $\gamma = 1/\sqrt{1 + \pi^2/16}$ with a value of $Q^b = -\sqrt{16/\pi^2 + 1} + 1$.
- [61] P. A. Ioselevich and M. V. Feigel'man, Anomalous Josephson current via Majorana bound states in topological insulators, *Phys. Rev. Lett.* **106**, 077003 (2011).
- [62] C. W. J. Beenakker, D. I. Pikulin, T. Hyart, H. Schomerus, and J. P. Dahlhaus, Fermion-parity anomaly of the critical supercurrent in the quantum spin-Hall effect, *Phys. Rev. Lett.* **110**, 017003 (2013).
- [63] Assuming a quasiparticle density of states $\rho_S(\epsilon) = 2/(\pi E_S) |\epsilon| \Theta(\epsilon^2 - \Delta^2) / \sqrt{\epsilon^2 - \Delta^2}$ from the superconducting electrodes, one can compute its contribution to Eq. (16) via $J_S(T) = \int_0^\infty d\epsilon \rho_S(\epsilon) \ln[\tanh(\frac{\epsilon}{2k_B T})]$, which yields Eq. (19), as detailed in Refs. [52,62].
- [64] B. A. Bernevig, T. L. Hughes, and S.-C. Zhang, Quantum spin Hall effect and topological phase transition in HgTe quantum wells, *Science* **314**, 1757 (2006).
- [65] M. König, S. Wiedmann, C. Brüne, A. Roth, H. Buhmann, L. W. Molenkamp, X.-L. Qi, and S.-C. Zhang, Quantum spin Hall insulator state in HgTe quantum wells, *Science* **318**, 766 (2007).
- [66] P. Sengupta, T. Kubis, Y. Tan, M. Povolotskyi, and G. Klimeck, Design principles for HgTe based topological insulator devices, *J. Appl. Phys.* **114**, 043702 (2013).
- [67] D. B. Topalovic, V. V. Arsooski, M. Z. Tadic, and F. M. Peeters, Asymmetric versus symmetric HgTe/Cd_xHg_{1-x}Te double

- quantum wells: Bandgap tuning without electric field, *J. Appl. Phys.* **128**, 064301 (2020).
- [68] S. Hart, H. Ren, M. Kosowsky, G. Ben-Shach, P. Leubner, C. Brüne, H. Buhmann, L. W. Molenkamp, B. I. Halperin, and A. Yacoby, Controlled finite momentum pairing and spatially varying order parameter in proximitized hgte quantum wells, *Nat. Phys.* **13**, 87 (2017).
- [69] H. Ren, F. Pientka, S. Hart, A. T. Pierce, M. Kosowsky, L. Lunczer, R. Schlereth, B. Scharf, E. M. Hankiewicz, L. W. Molenkamp, B. I. Halperin, and A. Yacoby, Topological superconductivity in a phase-controlled Josephson junction, *Nature (London)* **569**, 93 (2019).
- [70] Assuming, for example, the system from Ref. [69] with an induced superconducting gap of $\Delta \approx 64 \mu\text{eV}$, a Fermi velocity of $v_F = 5 \times 10^5 \text{ m/s}$, and a width of the junction of $\mathcal{W}_S = 1 \mu\text{m}$, we obtain $\gamma \approx 3.9$ for $B = 1 \text{ mT}$, showing that no excessively large magnetic fields are necessary to observe a sizeable SDE.
- [71] R. M. Lutchyn, J. D. Sau, and S. Das Sarma, Majorana fermions and a topological phase transition in semiconductor-superconductor heterostructures, *Phys. Rev. Lett.* **105**, 077001 (2010).
- [72] C.-K. Chiu and S. Das Sarma, Fractional Josephson effect with and without Majorana zero modes, *Phys. Rev. B* **99**, 035312 (2019).
- [73] D. Rainis and D. Loss, Majorana qubit decoherence by quasiparticle poisoning, *Phys. Rev. B* **85**, 174533 (2012).
- [74] P. Virtanen and P. Recher, Microwave spectroscopy of Josephson junctions in topological superconductors, *Phys. Rev. B* **88**, 144507 (2013).
- [75] D. Frombach and P. Recher, Quasiparticle poisoning effects on the dynamics of topological Josephson junctions, *Phys. Rev. B* **101**, 115304 (2020).
- [76] M. Mück and R. McDermott, Radio-frequency amplifiers based on dc SQUIDs, *Supercond. Sci. Technol.* **23**, 093001 (2010).